Synthesizing coherence loss by atmospheric turbulence in virtual microphone array signals

Dorothea Lincke, Timo Schumacher and Reto Pieren

Citation: The Journal of the Acoustical Society of America **153**, 456 (2023); doi: 10.1121/10.0016847
View online: https://doi.org/10.1121/10.0016847
View Table of Contents: https://asa.scitation.org/toc/jas/153/1
Published by the Acoustical Society of America

JASA ARTICLE

Synthesizing coherence loss by atmospheric turbulence in virtual microphone array signals

Dorothea Lincke,[1,a)] Timo Schumacher,[2] and Reto Pieren[1]
[1]Empa, Swiss Federal Laboratories for Materials Science and Technology, 8600 Dübendorf, Switzerland
[2]TU Berlin, Institute of Fluid Dynamics and Technical Acoustics, 10623 Berlin, Germany

ABSTRACT:
Phased microphone array methods are increasingly used to localize and quantify noise sources of aircraft under flight condition. However, beamforming results suffer from loss of image resolution and corruption of sound levels due to atmospheric turbulence causing coherence loss between microphones. A synthesis method is presented that reproduces these effects in a virtual environment. Sound propagation through turbulent atmosphere is described by models by Ostashev and Wilson and by von Kármán turbulence spectra. Spatial coherence is calculated based on the parabolic equation for statistically inhomogeneous, isotropic turbulence. Decorrelation of signals is achieved by time-varying mixing of mutually independent signals with identical PSD based on coherence factors. The concept of auralization is employed to account for propagation delay, geometrical spreading, Doppler effect, air absorption, and ground effect. The application is demonstrated for a virtual 56 m aperture microphone array. The impact of different meteorological conditions on the beamforming and deconvoluted results are presented. For increasing turbulence strength, the results show decreasing sound levels and increasingly blurred images. The proposed method allows us to reproduce the effects of turbulence-induced coherence loss in phased microphone array measurements and to optimize array designs and algorithms in a virtual, controllable environment.
 https://doi.org/10.1121/10.0016847
(Received 20 September 2022; revised 1 December 2022; accepted 13 December 2022; published online 23 January 2023)
[Editor: Vladimir E. Ostashev] Pages: 456–466

I. INTRODUCTION

Phased microphone arrays are able to detect moving sound sources at subsonic speed with beamforming techniques (Sijtsma, 2007). For aircraft, phased microphone array beamforming techniques offer the possibility to assess existing aircraft under flight condition. Therefore, the identification and quantification of noise emitting aircraft components is increasingly performed using microphone array methods (Merino-Martínez *et al.*, 2019). The aim of this publication is to present a new approach to study the effect of atmospheric turbulence on phased microphone array methods.

Although measurements under operational conditions have clear advantages over measurements on static test rigs, it is important to note that the complexity of the task is considerably increased because of uncontrolled experimental conditions. The degree of accuracy is dependent on meteorological conditions because of atmospheric turbulence effects and air absorption. Sound waves propagating through atmospheric turbulence are scattered by spatial and temporal fluctuations in wind and temperature. Scattered sound waves degrade the coherence in measured signals. Consequently, beamforming results suffer from loss of image resolution and a corruption of the sound levels in the source map (Merino-Martínez *et al.*, 2019). Partial loss of phase relation in phased microphone array measurements was investigated for open and closed wind tunnel experiments (Pires *et al.*, 2012), where decorrelation is caused by the turbulent shear layer and boundary layer, respectively. In case of sound propagation in atmospheric turbulence, the loss of coherence in a propagating acoustic wavefront and resulting variations in direction-of-arrival estimates have been studied theoretically (Collier and Wilson, 2003; Wilson, 1998).

Because of the uncertainties introduced by turbulent fluctuations in the atmosphere, flyover measurements are constrained to good weather conditions. Therefore, the atmospheric conditions during flyover measurements should satisfy the conditions mandatory for noise certification of aircraft defined by the International Civil Aviation Organization (2017).

The coherence loss of the measured signals can be partly compensated in a pre-processing step of the analysis. Microphones that are affected by coherence loss do not contribute effectively to the beamforming process but add noise to the source map instead. Selecting smaller sub-arrays then leads to lower background noise levels and increased peak levels. The size of the sub-arrays decreases with increasing analysis frequency (Michel *et al.*, 2004). The radius $R\,(\mathrm{m})$ of the effective aperture follows approximately the relation $R \approx V/f$, where $V = 4000\,\mathrm{m/s}$ is a constant and $f\,(\mathrm{Hz})$ the frequency (Sijtsma, 2007).

a)Electronic email: dorothea.lincke@empa.ch

Given that microphone array measurements of aircraft flyovers are very expensive in preparation and equipment, better understanding of the influence of turbulence-induced coherence loss in such measurements is highly desirable.

To this end, we present a method facilitating the optimization of existing procedures and the development of new ones minimizing the influence of coherence loss. The method is based on synthesized microphone array signals for purely virtual aircraft flyovers.

For synthesizing the virtual aircraft flyovers, we employ the concept of auralization. Auralization allows us to render simulated data audible (Vorländer, 2020). Auralization of aircraft noise has been used, among other purposes, as support of the aircraft design process and for communicating noise impact to stakeholders. A thorough overview of the field is given in Rizzi and Sahai (2019) and Rizzi *et al.* (2020). Recent publications have investigated possibilities to model coherence loss in ground effect for auralizations of aircraft flyovers measured with a single microphone (Arntzen and Simons, 2014; Forssén *et al.*, 2018; Pieren and Lincke, 2022; Rietdijk *et al.*, 2017). Ground effect is the interaction of direct sound and sound reflected from the ground (Attenborough and Renterghem, 2021). In the application discussed in this publication, the coherence loss between more than two microphones located on ground is targeted.

The method is tested using a simple virtual aircraft flyover with multiple sources and meteorological conditions. The results are analyzed with conventional beamforming in a first step, and an additional deconvolution step to improve the source localization. The analysis of the synthesized signals shows the above-mentioned effects of lower image resolution and corruption of the sound levels in the source map.

The paper is structured as follows: Sec. II provides theoretical background and the description of the synthesis. Section III demonstrates the application of the signal synthesis method to a virtual aircraft flyover and discusses beamforming and deconvolution results of the synthesized microphone array data. Section IV summarizes the article.

II. MODEL DESCRIPTION

The presented approach is based on recent theoretical formulations for sound propagation through the atmospheric boundary layer presented in Kamrath *et al.* (2021) and Ostashev *et al.* (2021). The presented model considers the propagation effects, propagation delay, geometrical spreading, Doppler effect, atmospheric absorption, ground effect, and coherence loss by atmospheric turbulence. The impact of atmospheric turbulence can be studied individually while keeping other factors constant. Additionally, the trajectory of the sound source is fully controllable. Random noise or ambient sounds can be added to the virtual microphone signals to study the impact of low signal-to-noise ratios, but is not further considered in this article.

Section II A introduces the geometry and geometrical assumptions of the virtual flyover. Section II B presents the computation of the coherence loss between different sensors of the microphone array. Section II C explains the mixing procedure to achieve partly decorrelated microphone signals. Section II D briefly summarizes the synthesis of non-turbulent propagation effects.

A. Sound path geometry for microphone array

Let the microphone array consist of M sensor positions distributed spatially on the ground. The monopole sound source travels at height h above ground and moves over the microphone array. The propagation distances between the source and the individual microphones are denoted by $\mathcal{L}_m$ with $m = 1, \ldots, M$.

Figure 1 shows the geometry of the sound propagation of a sound source for two microphones (mic 1 and mic 2) of the array. Line-of-sight propagation is assumed. The path lengths $\mathcal{L}_1, \mathcal{L}_2$ depend on the source height h and the elevation angles θ_1, θ_2 to the respective microphone. To compute the spatial coherence between two microphone sensors, we are interested in the lateral separation of the propagation paths at same range $\mathcal{L}$ from the sound source. The separation r_d is thus the projection of the real sound paths on the plane perpendicular to the propagation direction. Here, we define the propagation direction as the bisecting line between paths $\mathcal{L}_1$ and $\mathcal{L}_2$. The separation r_d is then determined as the length of the line that intersects $\mathcal{L}_1$ and $\mathcal{L}_2$ each at the distance $(\mathcal{L}_1 + \mathcal{L}_2)/2$ from the sound source.

In the following derivations, it is assumed that the coherence loss in longitudinal direction is much smaller than in lateral direction and is therefore omitted. For $\Delta\theta = |\theta_2 - \theta_1| > 0$, the propagation paths to the individual microphones do not have the same length ($\mathcal{L}_1 \neq \mathcal{L}_2$) but fulfill

$$r_d \ll \min(\mathcal{L}_1, \mathcal{L}_2). \tag{1}$$

If Eq. (1) is not fulfilled, the proposed method will overestimate the signal coherence. Higher accuracy could be achieved by additionally considering the transverse-longitudinal coherence function, which does not neglect coherence loss in longitudinal direction. A derivation of the transverse-longitudinal coherence function for plane waves is presented in Ostashev *et al.* (2009).

B. Atmospheric turbulence model leading to characterization of coherence loss

For any two microphones of the microphone array, let $p(\mathbf{R}, t')$ be the real-valued sound pressure at position $\mathbf{R} = (x, y, z)$ with the short-time Fourier transform (STFT)

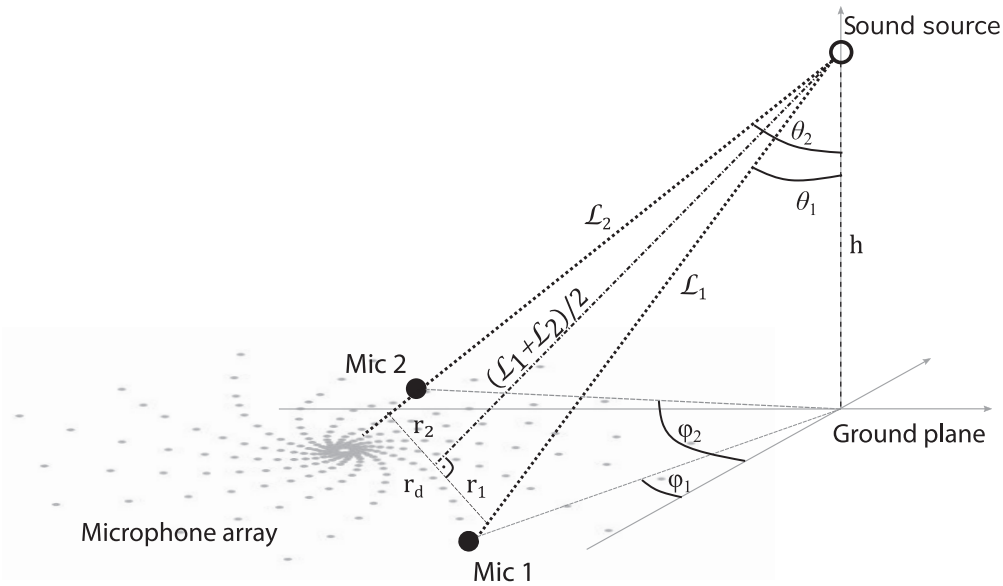

FIG. 1. Geometry source-microphone sound propagation. Microphone array indicated by light gray dots.

$$\hat{p}(\mathbf{R},\omega,t)=\frac{1}{2\pi}\int_{-\infty}^{\infty}p(\mathbf{R},t')w(t'-t)e^{-j\omega t'}dt', \tag{2}$$

where ω is the angular frequency and w is a window function.

Assuming Eq. (1), we denote the positions of the microphones as $\mathbf{R}_1=(\mathcal{L},\mathbf{r}_1)$ and $\mathbf{R}_2=(\mathcal{L},\mathbf{r}_2)$, where $\mathbf{r}_1$ and $\mathbf{r}_2$ are the lateral distances perpendicular to the joint propagation path as explained in Sec. II A. The mutual coherence function or cross-spectrum of two signals at the same distance $\mathcal{L}$, at different time instances t_1, t_2, and frequencies ω_1, ω_2 is defined as

$$\begin{aligned}&\Gamma(\mathcal{L};\mathbf{r}_1,\omega_1,t_1;\mathbf{r}_2,\omega_2,t_2)\\&\quad=\langle\hat{p}(\mathcal{L},\mathbf{r}_1,\omega_1,t_1)\hat{p}^*(\mathcal{L},\mathbf{r}_2,\omega_2,t_2)\rangle.\end{aligned} \tag{3}$$

The angle brackets $\langle\rangle$ indicate the ensemble average. The asterisk (*) denotes the complex conjugate.

In the following, we set $\omega_1=\omega_2$ and $t_1=t_2$ and omit these in the notation, because we focus on spatial coherence. We therefore neglect cross-frequency coherence and temporal coherence.

In case of a non-turbulent atmosphere, the mutual coherence function is denoted as $\Gamma_0(\mathcal{L},r_d)$. We can then define the coherence factor C_{coh} as the normalized mutual coherence function,

$$C_{\text{coh}}=\frac{\Gamma(\mathcal{L};r_d)}{\Gamma_0(\mathcal{L};r_d)}. \tag{4}$$

The remainder of this section presents the computation of the coherence factor C_{coh} based on Ostashev *et al.* (2021). The computation of the coherence is based on the narrow-angle parabolic equation. In case of statistically inhomogeneous isotropic turbulence, the mutual coherence function of a spherical sound wave for vertical or slanted line-of-sight propagation is given as

$$\begin{aligned}C_{\text{coh}}(\mathcal{L};r_d)=\exp\Bigg\{&-\frac{\pi^2k_0^2}{\cos\theta}\int_0^h dz\int_0^\infty\Phi_{\text{eff}}(z,\kappa)\\&\times\left[1-J_0\left(\frac{\kappa z r_d}{h}\right)\right]\kappa\,d\kappa\Bigg\},\end{aligned} \tag{5}$$

where $\mathcal{L}=h/\cos\theta$, $k_0=\omega/c_0$ is the reference acoustical wavenumber in air for the reference sound speed c_0, κ is the turbulence wavenumber, J_0 is the Bessel function of the first kind and zero order, and Φ_{eff} is the effective turbulence spectrum.

For the characterization of atmospheric turbulence, we employ the von Kármán turbulence spectrum. The von Kármán turbulence spectrum is based on parametrizations of temperature and wind velocity fluctuations in the atmospheric boundary layer (ABL),

$$\begin{aligned}\Phi_{\text{eff}}(z,\kappa)=\frac{\Gamma(11/6)}{\pi^{3/2}\Gamma(1/3)}\Bigg[&\frac{\sigma_T^2(z)L_T^3(z)}{T_0^2\left(1+\kappa^2L_T^2(z)\right)^{11/6}}\\&+\frac{22}{3}\frac{\sigma_{v,s}^2L_{v,s}^5(z)\kappa^2}{c_0^2\left(1+\kappa^2L_{v,s}^2(z)\right)^{17/6}}\\&+\frac{22}{3}\frac{\sigma_{v,b}^2L_{v,b}^5\kappa^2}{c_0^2\left(1+\kappa^2L_{v,b}^2\right)^{17/6}}\Bigg],\end{aligned} \tag{6}$$

where $\Gamma(n)=(n-1)!$ is the Gamma function (not to be confused with the mutual coherence function), and T_0 is the mean temperature near the ground.

As suggested by Ostashev and Wilson (2016) and Kamrath *et al.* (2021), the variances of temperature σ_T^2, shear-produced wind velocity fluctuations $\sigma_{v,s}^2$, and buoyancy-produced wind velocity fluctuations $\sigma_{v,b}^2$ are

https://doi.org/10.1121/10.0016847

parameterized based on the turbulence scaling parameters: friction velocity u_*, surface heat flux Q_H, boundary layer height z_i, and Obukhov length L_o using the following expressions:

$$\sigma_T^2 = \frac{4T_*^2}{[1-10z/L_o]^{2/3}},$$
$$\sigma_{vs}^2 = 3u_*^2,$$
$$\sigma_{vb}^2 = 0.35w_*^2. \quad (7)$$

Here, $T_* = -Q_H/\rho_0 c_p u_*$ is the surface layer temperature scale, $w_* = (z_i g Q_H/\rho_0 c_p T_0)^{1/3}$ the convection velocity scale, and $L_o = -u_*^3 T_s \rho_0 c_p/(g\kappa_v Q_H)$ is the Obukhov length. The parameters ρ_0, c_p, and g, describe the air density, specific heat and gravitational acceleration.

The effective turbulence spectrum $\Phi_{\text{eff}}(z,\kappa)$ in Eq. (6) becomes inhomogeneous in the vertical direction by accounting for the height dependence of the length scales of turbulence. The length scales of turbulence are described by Monin–Obukhov similarity theory (MOST) and mixed-layer similarity theory and given by

$$L_T(z) = 2z\frac{1-7z/L_o}{1-10z/L_o},$$
$$L_{v,s}(z) = 1.8z,$$
$$L_{v,b} = 0.23z_i. \quad (8)$$

C. Noise mixing

1. Computation of coherence matrix

Following the theoretical descriptions in Sec. II B, the coherence factor C_{coh} is computed for every microphone pair by numerical integration of Eq. (5). The integration is performed for turbulence wavenumbers $\kappa = 10^{-4}\,\text{m}^{-1}$ to $10^2\,\text{m}^{-1}$ on a logarithmic scale. The numerical integration is performed with the implementation of Simpson's rule in the Python library SciPy (Virtanen *et al.*, 2020). The required sound path lengths $\mathcal{L}$ and the lateral separations r are determined as presented in Sec. II A. The resulting coherence factors yield a symmetrical coherence matrix $\mathbf{C}_{\text{coh}}$ of $M \times M$ factors. C_{coh} is discretized in frequency and time leading to a four-dimensional representation $\mathbf{C}_{\text{coh}}(l,\omega_k)$ of size $M \times M \times L \times K$ with $l = 1,\ldots,L$ time steps, and $k = 1,\ldots,K$ discrete frequency bins.

2. Mixing of independent noise signals

Figure 2 depicts the procedure for generating M nonstationary, mutually partly coherent signals.

In a first step, M mutually independent time domain noise signals are created with a random number generator. The signals are designed to have the same power spectral densities (PSD). The signals are transformed to frequency domain by the short-time Fourier transform (STFT) leading to M mutually independent complex random signals

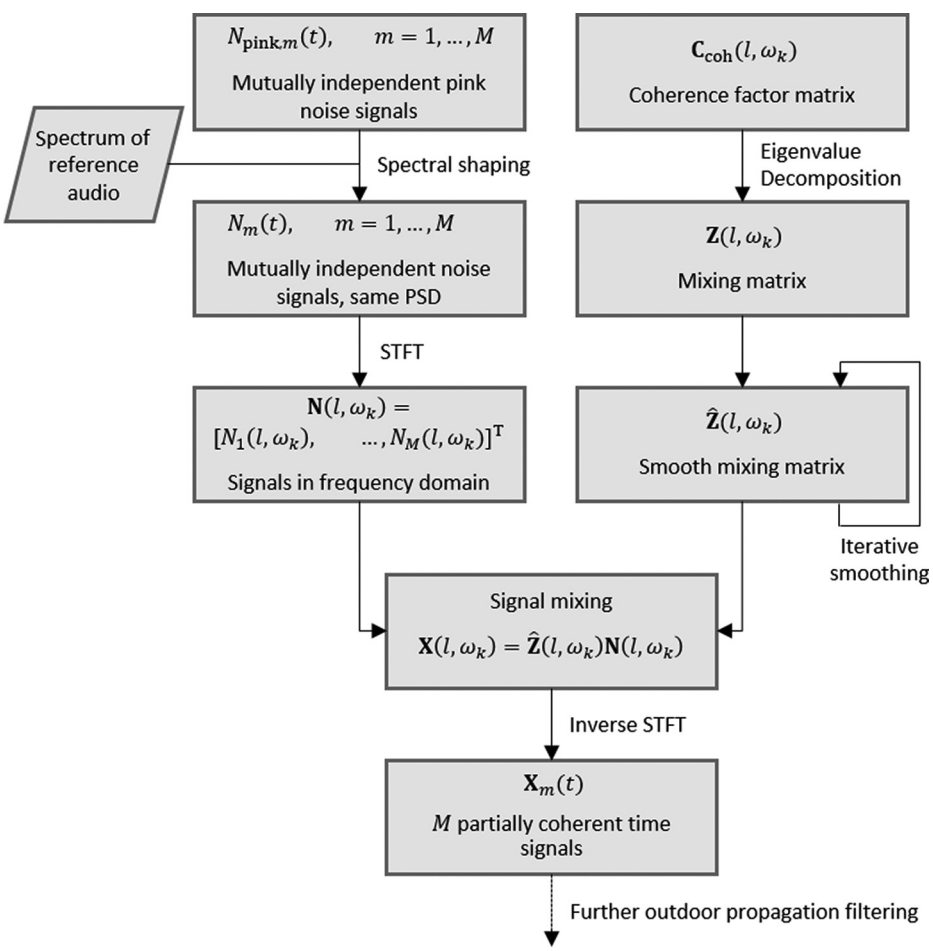

FIG. 2. Block diagram showing the processing steps to generate virtual microphone signals described in Sec. II C 2.

$\mathbf{N}(l,\omega_k) = [N_1(l,\omega_k),\ldots,N_M(l,\omega_k)]^T$. The STFT is performed with a Hann window of 2048 samples in length and 50% overlap.

The frequency-dependent and time-varying coherence between the microphone signals is created by mixing the STFT coefficients of the independent noise signals based on the description in Habets *et al.* (2008). The desired STFT coefficients $\mathbf{X}(l,\omega_k)$ of the microphone array are obtained by

$$\mathbf{X}(l,\omega_k) = \mathbf{Z}^H(l,\omega_k)\mathbf{N}(l,\omega_k), \tag{9}$$

where $\mathbf{Z}(l,\omega_k)$ represents the mixing matrix and $(.)^H$ the Hermitian operation. The mixing matrix is calculated by Cholesky decomposition or eigenvalue decomposition (EVD) of the coherence factor matrix. The Cholesky decomposition can only be calculated if the matrix $\mathbf{C}_{\mathrm{coh}}(l,\omega_k)$ is positive definite. This requirement is not necessarily fulfilled because of the assumptions explained in Sec. II A, namely the geometrical assumption $r_d \ll \min(\mathcal{L}_1,\mathcal{L}_2)$ and the neglect of coherence loss in longitudinal direction. The EVD offers a more general solution that can deal with non-positive definite matrices. The EVD of the coherence factor matrix is

$$\mathbf{C}_{\mathrm{coh}}(l,\omega_k) = \mathbf{V}(l,\omega_k)\mathbf{D}(l,\omega_k)\mathbf{V}^H(l,\omega_k), \tag{10}$$

where $\mathbf{V}(l,\omega_k)$ is the matrix containing the eigenvectors and $\mathbf{D}(l,\omega_k)$ is a diagonal matrix with the corresponding eigenvalues. The diagonal matrix can be split up to obtain

$$\mathbf{C}_{\mathrm{coh}}(l,\omega_k) = \mathbf{V}(l,\omega_k)\sqrt{\mathbf{D}(l,\omega_k)}\sqrt{\mathbf{D}(l,\omega_k)}\mathbf{V}^H(l,\omega_k). \tag{11}$$

The mixing matrix is then (Habets *et al.*, 2008)

$$\mathbf{Z}(l,\omega_k) = \sqrt{\mathbf{D}(l,\omega_k)}\mathbf{V}^H(l,\omega_k). \tag{12}$$

In a recent publication, the method was extended to improve spectral smoothness and the mix balance (Mirabilii *et al.*, 2021). Low spectral smoothness describes discontinuities between adjacent discrete frequency bins ω_k of the mixing matrices. Calculation of the mixing matrices by Cholesky decomposition leads to better spectral smoothness of the mixing matrices than the EVD, which is used for this publication. A mixing matrix yields a balanced mix, if each output signal consists of a similar mix of input signals. While the mix balance does not influence the results in this paper due to the Gaussian nature of the signals, enhancement of spectral smoothness yields improved results for the presented application. To improve spectral smoothness of the mixing matrices, Mirabilii *et al.* (2021) suggest to choose adjacent frequency bands such that they are as similar as possible by minimizing

$$\epsilon = \frac{1}{K}\sum_k ||\mathbf{Z}(\omega_k) - \mathbf{Z}(\omega_{k-1})||_{\mathrm{F}}^2, \tag{13}$$

where $||\cdot||_F$ denotes the Frobenius norm of a matrix.

Following the suggested procedure in Mirabilii *et al.* (2021), Eq. (13) is minimized iteratively to improve spectral smoothness of the mixing matrices: The smooth mixing matrix at the kth frequency bin is computed by

$$\hat{\mathbf{Z}}_{\mathrm{f}}(\omega_k) = \hat{\mathbf{U}}_{\mathrm{f}}(\omega_k)\mathbf{Z}(\omega_k). \tag{14}$$

Here, $\hat{\mathbf{U}}_{\mathrm{f}}$ is given by

$$\hat{\mathbf{U}}_{\mathrm{f}}(\omega_k) = \mathbf{W}\mathbf{T}^{\mathrm{H}}, \tag{15}$$

where $\mathbf{W}$ and $\mathbf{T}$ represent the unitary matrices containing the left-singular and right-singular vectors of $\mathbf{R} = \mathbf{Z}(\omega_{k-1})\mathbf{Z}(\omega_k)^{\mathrm{H}}$ and are obtained by the singular value decomposition (SVD)

$$\mathbf{R} = \mathbf{W}\Sigma\mathbf{T}^{\mathrm{H}}. \tag{16}$$

Equation (14) is computed iteratively for all frequency indices $\hat{k}$. We first determine the smooth mixing matrix for $\hat{k} = 1$ and continue with $\hat{k} = 2$, etc.

The smooth mixing matrix $\hat{\mathbf{Z}}(l,\omega_k)$ and the STFT coefficients $\mathbf{N}(l,\omega_k)$ are inserted in Eq. (9) to yield the STFT coefficients of the sensor signals. Finally, the time signals are obtained by calculating the inverse STFT of $\mathbf{X}(l,\omega_k)$.

D. Synthesis of non-turbulent propagation effects

Non-turbulent propagation effects are simulated by applying time domain filters to the signals $\mathbf{x}(t)$. Time-variant filters are designed following the method for aircraft auralization described in Pieren *et al.* (2019). The propagation filtering is performed individually for each sound source–microphone pair considering the respective source–receiver geometry.

The propagation delay and the Doppler frequency shift are realized by a fractional delay filter. Because of the fractional delays, the new samples must be interpolated. Linear interpolation causes distortions due to aliasing, thus, we use a windowed sinc interpolation (Laakso *et al.*, 1996). To account for geometrical spreading of a point source, the sound pressure is multiplied by $1/\mathcal{L}$, where $\mathcal{L}$ is the sampled distance between source and receiver. Air attenuation is considered by designing a minimum-phase finite impulse response (FIR) filter based on the absorption coefficient α which is determined through (ISO 9613–1:1993, 1993). Vertical profiles of the absorption coefficient due to e.g., a temperature gradient, can be considered. If the virtual microphones are placed directly on an acoustically hard ground, the reflection modelling is replaced by pressure doubling.

Bending of sound paths by temperature gradients or convection is not considered, as the effect is negligible for mainly vertical sound propagation. Typical flyover measurements are conducted with aircraft traveling at up to a few hundred meters height above ground and for elevation angles between 50° and 130°. Advection of sound paths by wind can easily be considered and accounted for in purely

https://doi.org/10.1121/10.0016847

virtual setups with known wind profiles, but is not included in this article.

III. APPLICATION EXAMPLE

The application of the method is demonstrated for a large, horizontal phased microphone array and two source configurations, each in four different meteorological conditions.

A. Virtual setup

The virtual microphone array consists of 238 sensors located in accordance with the microphone array measurements by the German Aerospace Center (DLR) described in Siller *et al.* (2020) and Siller *et al.* (2021). The aperture of the microphone array is 56 m. The microphones are located directly on the runway.

Figure 3 illustrates the sources flying over the microphone array. Source configuration I consists of two independent monopole sources (labeled A and B) moving along a common trajectory at 2 m distance. Source configuration II consists of two sources at 4 m distance along the same trajectory. The leading source B moves from (x,y) = (−100 m, 20 m) to (x,y) = (100 m, 20 m) at 180 m height and at velocity v = 88 m/s. Source A follows source B on the same trajectory and with the same speed with the respective distance to source B. The distances are chosen such that the source separation in the beamforming results are expected to exhibit clear impairment at 1 kHz for the smaller distance, and moderate impairment for the larger distance, if coherence loss by atmospheric turbulence is considered.

The directivity, which typically occurs with aeroacoustic sources, is neglected by the modelling through monopoles. However, this investigation mainly focuses on the separation of sources, which can be shown in this simplified approach. Since only a short interval is considered in the subsequent source localization step, we do not expect that modelling a directivity would impact the presented results, while greatly increasing the complexity of the approach.

For each sound source, 238 mutually independent broadband source signals are synthesized corresponding to 238 microphones. The synthesized signals consist of spectrally shaped pink noise with sampling frequency $f_s = 48\,\mathrm{kHz}$. The spectrum used as a template for the synthesized sounds is based on the power spectral density of a real-world flyover measurement with the above-mentioned microphone array. The duration of the synthesized signal is approximately 3 s.

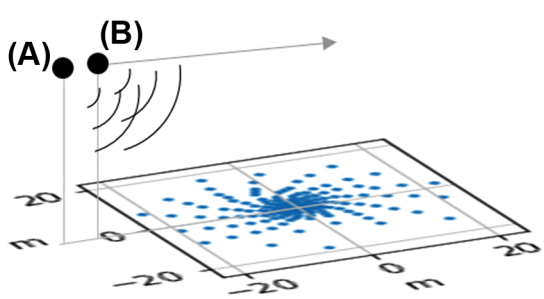

FIG. 3. (Color online) Virtual test case: Two point sources (labeled A and B) moving at the same speed along x axis above a planar 238 microphone array.

B. Virtual meteorological conditions

The application is demonstrated for four different meteorological conditions characterized by different degrees of atmospheric turbulence. Low wind conditions are characterized by friction velocity $u_* = 0.1\,\mathrm{m/s}$, strong wind leading to shear-generated turbulence by $u_* = 0.5\,\mathrm{m/s}$. Low solar radiation with low buoyancy-produced turbulence is characterized by surface sensible heat flux $Q_H = 50\,\mathrm{W/m^2}$ and $z_i = 500\,\mathrm{m}$. Strong solar radiation causing buoyancy-produced turbulence and leading to large boundary layer heights z_i is characterized by $Q_H = 200\,\mathrm{W/m^2}$ and $z_i = 2000\,\mathrm{m}$. These values are typical for sunny summer afternoons. The combination of these values leads to the four conditions shown in Table I.

For easier comparison of the turbulence effect, the non-turbulent parameters are kept constant among all conditions. Mean temperature and surface temperature are $T_0 = T_s = 15\,^\circ\mathrm{C}$. This may not be realistic in many cases, but the effect of the temperature difference on C_{coh} is small compared to the turbulence scaling parameters. Relative humidity is $rh = 70\,\%$.

Equations (5) and (6) indicate that the magnitude of the coherence factor C_{coh} is dependent on three atmospheric turbulence production mechanisms, namely temperature fluctuations, shear-produced wind velocity fluctuations, and buoyancy-produced wind velocity fluctuations.

Figure 4 presents the respective contribution of the turbulence production mechanism to the coherence factor. The temperature fluctuations have a negligible influence on C_{coh}. In case of low wind, hence, low shear-produced turbulence, the coherence loss is primarily caused by buoyancy-produced wind velocity fluctuations. For overcast days and strong wind corresponding to Fig. 4(c), shear-produced wind velocity fluctuations dominate the coherence loss. For both strong wind and strong solar radiation, the magnitude of the coherence loss depends on both turbulence production mechanisms.

C. Noise mixing application

Partial correlation of the virtual microphone signals is achieved by mixing the 238 mutually independent synthesized signals with a sampling rate of 48 kHz as explained in

TABLE I. Turbulence scaling parameters for conditions (a)–(d).

Condition	(a)	(b)	(c)	(d)
u_* (m/s)	0.1	0.1	0.5	0.5
Q_H (W/m^2)	50	200	50	200
z_i (m)	500	2000	500	2000

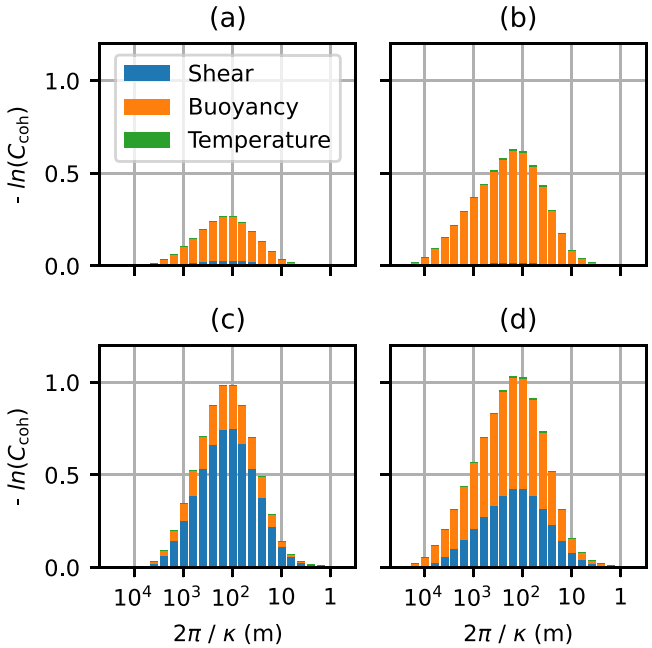

FIG. 4. (Color online) Stacked contributions of shear-produced and buoyancy-produced wind velocity fluctuations and temperature fluctuations to $C_{\mathrm{coh}}(f = 1\,\mathrm{kHz})$ based on Eqs. (5) and (6) for turbulence conditions presented in Table I. Geometry of propagation: Source at $h = 180$ m height directly above the receivers. Receivers at 10 m distance from each other. Contributions due to temperature fluctuations are hardly visible.

Sec. II C. The STFT coefficients of the signals are computed with a FFT size of $N = 2^{11}$ samples, a 50% overlap, and a Hann windowing function. The resulting time discretization and consequently update frequency of the decorrelation is 46 Hz corresponding to 21 ms duration per segment.

Figure 5 compares the theoretical curve of the coherence factor C_{coh} and the coherence of the synthesized signals for two microphones of the array with a sound path separation of $r_d = 0.54$ m. To demonstrate the agreement between target coherence and coherence of the synthesized signals, Fig. 5 shows the simulation of a non-moving, stationary

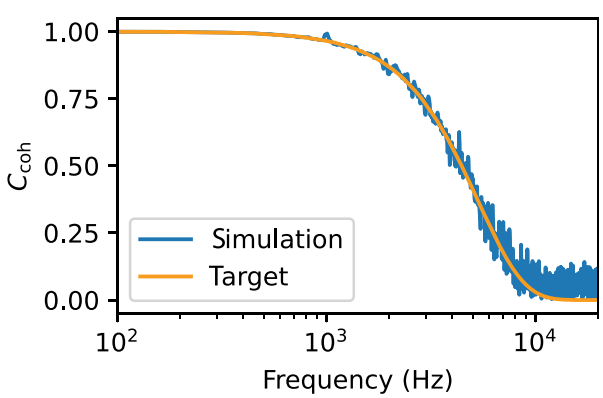

FIG. 5. (Color online) Comparison of target coherence C_{coh} and coherence of synthesized signals of a static sound source located at 180 m above the microphones with maximum sound path separation $r_d = 0.54$ m. Turbulence parameters: $u_* = 0.3$ m/s, $Q_H = 150\,\mathrm{W/m^2}$, $z_i = 1500$ m. The signal coherence of the simulation was estimated using Welch's method with a FFT size of $N = 2^{11}$ samples, a Hann windowing function, and 50% overlap.

sound source. Aside from random coherence fluctuations in the synthetic signal, the simulation allows us to reproduce the theoretical values over the whole frequency range very well.

D. Analysis of virtual test cases

The synthesized microphone array signals are analyzed with conventional delay-and-sum beamforming (CBF). Delay-and-sum beamforming is a fast and intuitive method (Merino-Martínez *et al.*, 2019) that uses the propagation time difference between microphones to focus on an assumed source point. This suppresses signals emitted from sources that are not located close to the focus point. The fundamental idea of CBF can be applied in time as well as in frequency domain. Here, the time domain is used, as it can be easily extended to moving focus points (Michel and Möser, 2009).

CBF in time domain is expressed as (Piet *et al.*, 2002)

$$b(t) = \frac{1}{M}\sum_{m=1}^{M} \mathcal{L}_m p_m(t + \mathcal{L}_m/c), \tag{17}$$

where $b(t)$ is the reconstructed time signal at a focus point.

Typically, Eq. (17) is evaluated repeatedly for a set of points in the region where sources are expected to occur. Here, the focus points are located on a 20×20 m grid at the height of the sound sources with a regular spacing of 0.2 m. The grid follows the movement of the sound sources. For each grid point, the time signal $b(t)$ is calculated and transformed into a one-third octave band spectrum. The results are then displayed in source maps corresponding to the evaluated region. The signal duration used in the analysis is approximately 0.4 s, corresponding to a distance travelled by the sources of 31.6 m, centered vertically above the array.

Figures 6 and 7 present the CBF results of the virtual test cases. For each source configuration, the one-third octave bands at 1 kHz (left column) and 2 kHz (right column) are shown. The first row of subfigures titled *coherent* presents the beamforming analysis of the simulation without consideration of turbulence-induced coherence loss. Rows labeled (a)–(d) correspond to the turbulence conditions presented in Table I.

Expected effects of atmospheric turbulence on phased microphone array measurements include the loss of image resolution and a corruption of the sound levels in the source maps (Merino-Martínez *et al.*, 2019). The first effect is most apparent in Fig. 6, showing the analyzed virtual test cases for a source separation of 2 m for the one-third octave band with center frequencies $f_c = 1$ kHz and $f_c = 2$ kHz. The localization of the sources is blurred. Especially for conditions (b)–(d), the source map with center frequency $f_c = 1$ kHz indicate only one source at the center of the map. The second effect is apparent in all virtual test cases. For both source configurations, the sound levels of the source maps decrease when coherence loss is considered in the test

https://doi.org/10.1121/10.0016847

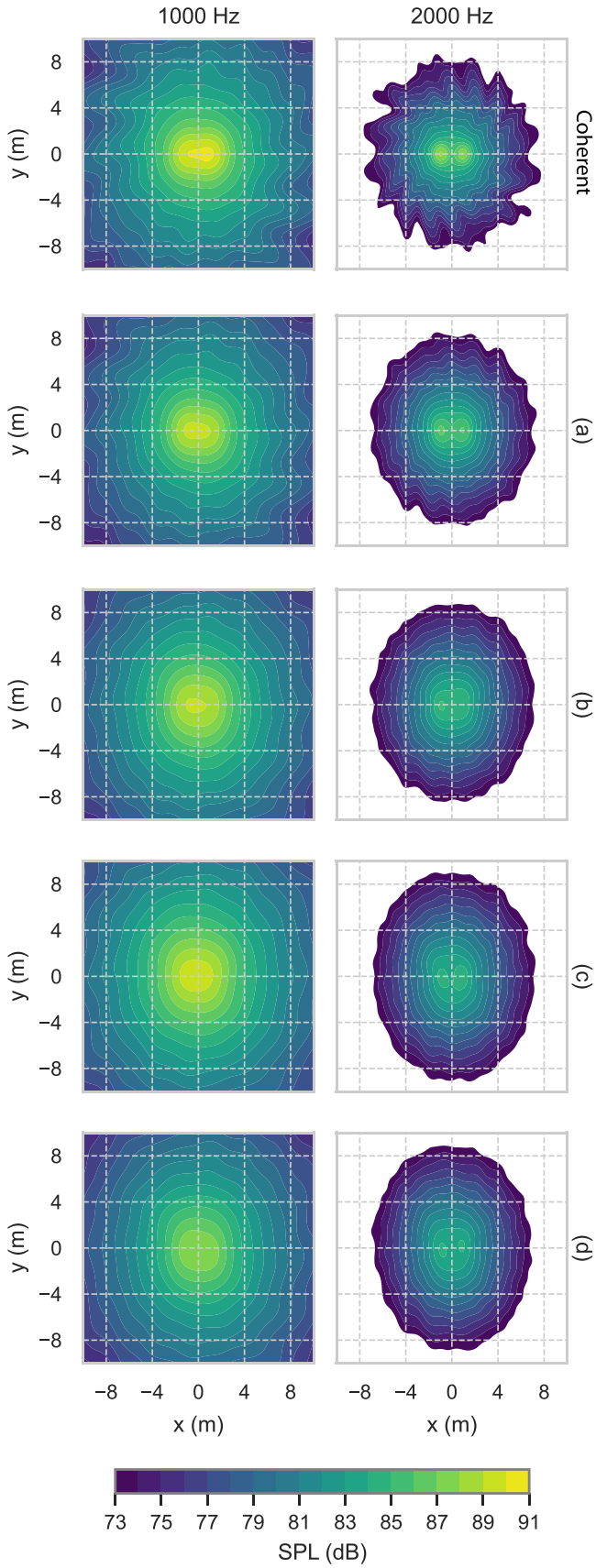

FIG. 6. (Color online) Beamforming source maps for 2 m source separation. Non-turbulent condition labeled *coherent*, turbulent conditions (a)–(d). For the respective condition, 1 kHz (left column) and 2 kHz (right column) one-third octave bands are shown.

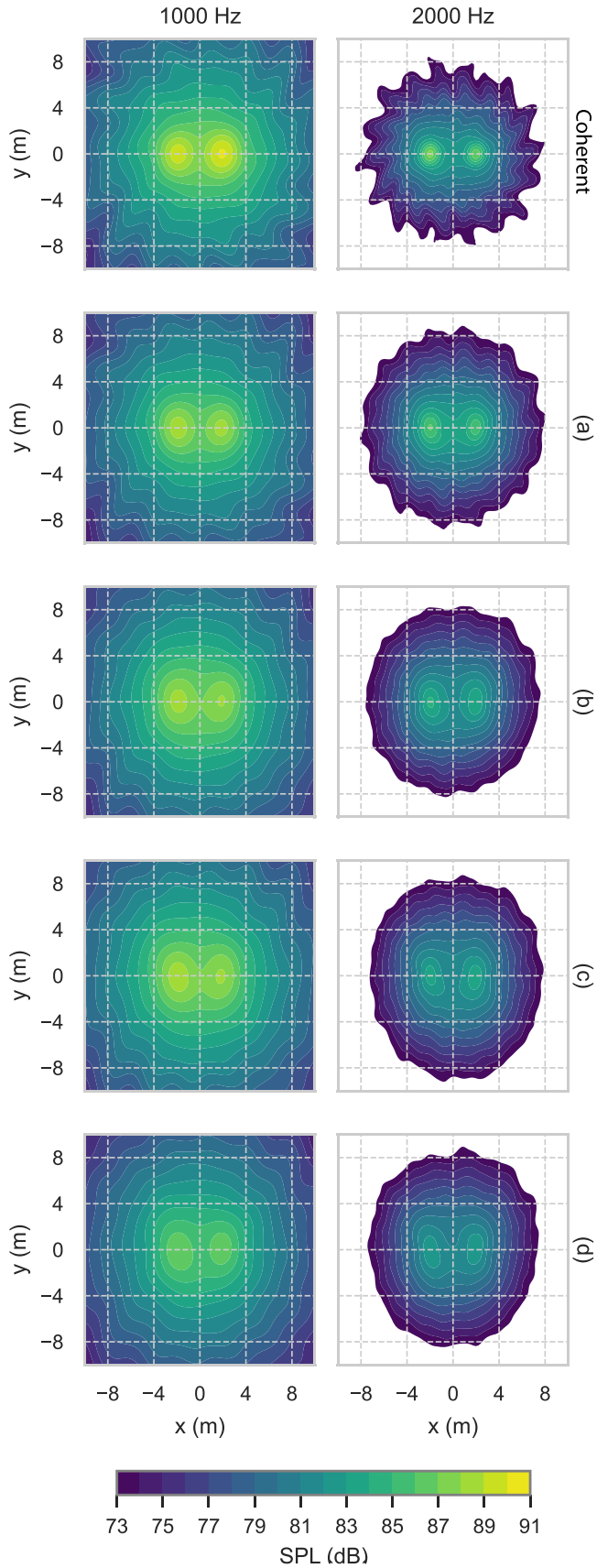

FIG. 7. (Color online) Beamforming source maps for 4 m source separation. Non-turbulent condition labeled *coherent*, turbulent conditions (a)–(d). For the respective condition, 1 kHz (left column) and 2 kHz (right column) one-third octave bands are shown.

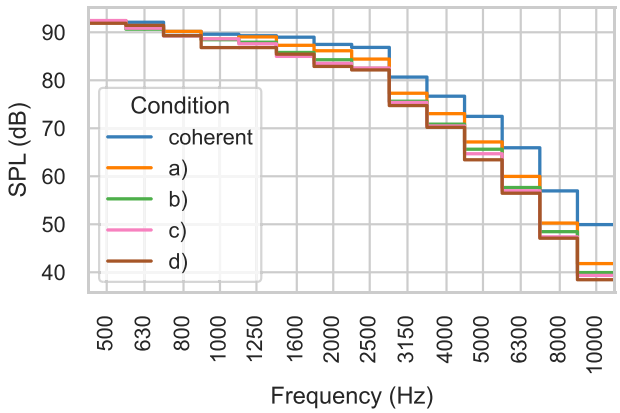

FIG. 8. (Color online) SPL spectrum at the position of the trailing source in beamforming source maps for 4 m source separation. The spectrum for the leading source is mostly identical and not shown here.

case. This visual impression is confirmed by Fig. 8 showing the sound pressure level (SPL) per one-third octave band at the source position in the beamforming source maps. For frequency bands at 1 kHz and higher, the virtual test case without loss of coherence shows consistently higher values of SPL per one-third octave band than the other simulations. Condition (a), corresponding to the lowest turbulence strength, leads to higher SPL values than the remaining conditions. The spectra for conditions (b)–(d) are very similar, with condition (b) (low friction velocity–high surface heat flux) still having slightly higher values.

The delay-and-sum approach within the beamforming algorithm assumes coherent sound propagation. Atmospheric turbulence leads to partly randomized phases of the complex signals. Consequently, delaying the signals does not lead to in-phase summation. Instead, part of the signal is summed energetically, leading to an underestimation of the signal levels.

As can be seen in the source maps in Figs. 6 and 7, the delay-and-sum approach generally suffers from a poor spatial resolution. The energy of acoustic sources is spread across an extensive region of the source map. This holds true especially for low frequencies. This spread depends on the distance and direction of the source relative to the microphone array, as well as the number and locations of the microphones. For points sources, this is described in the so called point-spread-function (PSF), which can be estimated for each focus point on the grid.

Based on the PSF, the source maps can be enhanced by Deconvolution Approach for the Mapping of Acoustic Sources (DAMAS) (Brooks and Humphreys, 2006). Guérin and Weckmüller have extended the approach to moving sources (Guérin and Weckmüller, 2008; Guérin *et al.*, 2006). This method was successfully applied to flyover microphone array measurements (Guérin and Siller, 2008; Ishii *et al.*, 2014; Siller *et al.*, 2021).

Figure 9 presents source maps obtained by the deconvolution of the beamforming results. Here, only the source configuration for 2 m distance is shown, as the sources remain clearly distinct for all turbulence conditions. Similar

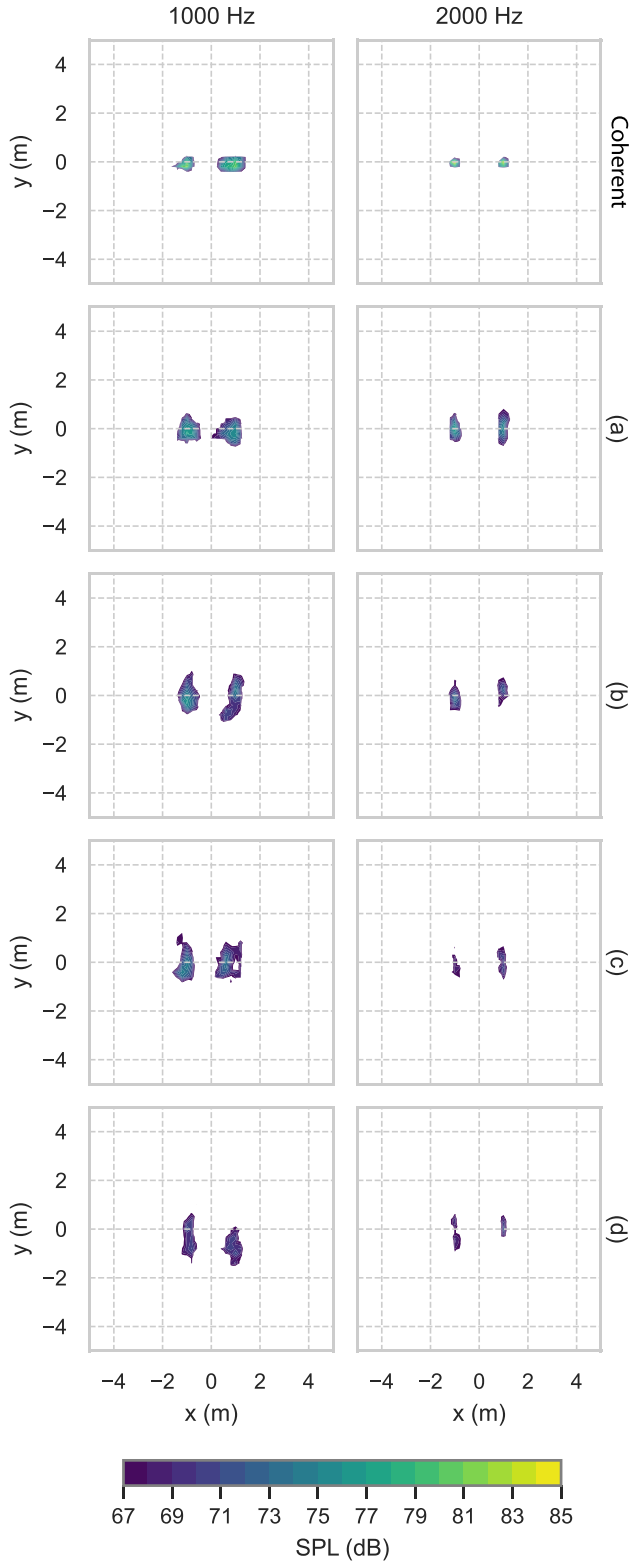

FIG. 9. (Color online) Source maps after deconvolution step for source separation of 2 m and one-third octave bands 1 and 2 kHz. Note the different scaling compared to Figs. 6 and 7.

to Figs. 6 and 7, the underestimation of the sound levels is apparent for increasing strength of atmospheric turbulence.

The applied deconvolution allows us the integration of the source strengths of a region. Figure 10 displays the

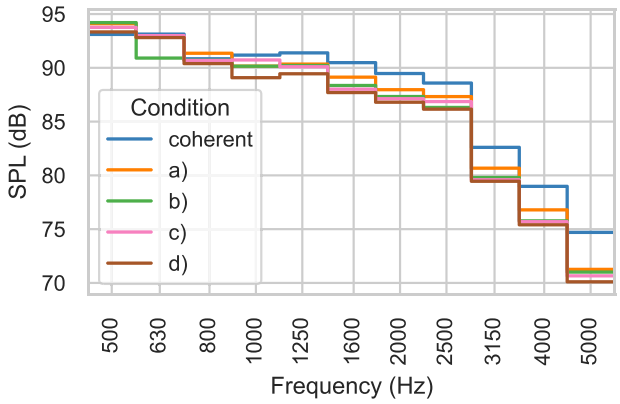

FIG. 10. (Color online) Integrated total energy of deconvoluted source map (covering both sources) as spectrum.

integrated total energy for the deconvoluted source maps. Thus, both sources are located within the integration area. As in Fig. 8, the total energy is highest for the simulation without coherence loss. Turbulence conditions (a)–(d) lead to decreasing levels of sound pressure.

The analysis reveals that the expected effects on phased microphone array measurements, caused by coherence loss due to atmospheric turbulence, could be reproduced using the virtual test cases.

IV. CONCLUSION

This article presents a method to synthesize coherence loss by atmospheric turbulence in phased microphone array measurements. The aim of the method is to provide a virtual environment for the study and optimization of localization methods for moving sound sources like aircraft and to assess the influence of the given meteorological conditions during a measurement on the beamforming results.

The atmospheric boundary layer was modeled based on MOST and mixed-layer similarity theory. Therefore, the method is best applicable to non-neutral boundary layers and ideally flat terrain. Atmospheric turbulence was represented with von Kármán turbulence spectra. Frequency-dependent coherence factors between all microphone combinations of the array were modeled based on the narrow-angle parabolic equation for statistically inhomogeneous, isotropic turbulence. Coherence loss was considered as purely spatial coherence loss. Temporal or cross-frequency coherence loss was not considered. Further, transversal coherence loss was neglected, as lateral coherence loss dominates.

Coherence factors were repeatedly computed to account for source motion assuming slowly varying values for C_{coh}. Based on the coherence factors, the mixing matrix was calculated by an EVD. To simulate partly correlated microphone signals, a number of mutually independent signals with identical power spectral density was created. The coherence loss between microphones was subsequently recreated by a matrix multiplication of the STFT coefficients of the uncorrelated signals with the mixing matrix. After creating the decorrelated signals, further propagation filtering was applied to account for propagation delay, geometrical spreading, Doppler effect, air attenuation, and ground reflection.

The method was demonstrated for four different meteorological conditions characterized by varying values of friction velocity, surface sensible heat flux, and boundary layer height. Virtual test cases of aircraft flyover measurements were simulated for two idealized moving monopole sound sources passing a large, phased microphone array. So far, line sources can not be considered. Directivity of the aeroacoustic sources was neglected. Line-of-sight sound propagation was assumed. For a known mean wind profile, advection of sound paths can be easily accounted for, but has not been considered in this publication.

The analysis showed that the expected effects caused by coherence loss due to atmospheric turbulence were successfully reproduced. Source maps of beamforming analyses and deconvoluted source maps showed an underestimation of sound pressure levels and blurred images. The localization is less accurate if atmospheric turbulence is considered. In case of the beamforming results, this led partly to indistinguishable sound sources for $f = 1$ kHz and $f = 2$ kHz at a source separation of 2 m. The deconvoluted results show clear source distinction for monopole sources at 2 m separation, but the source maps still exhibit underestimation of the sound levels by several decibels.

The developed virtual environment will facilitate the further optimization of phased microphone array methods for outdoor applications like aircraft flyover measurements. Future work will focus on applying the presented method to virtual test cases that closer represent aircraft flyover measurements by considering arrangement and characteristics of the aeroacoustics sources of aircraft. Such sources include engine noise, which is dominating during takeoff, as well as airframe noise and landing gear noise during the final descent. This will allow a more in depth investigation of the ability of evaluation methods to correctly localize and quantify sources under varying atmospheric conditions. The presented work is a first step towards the identification of well-founded limits for atmospheric conditions during flyover measurements, that guarantee good reproducibility.

ACKNOWLEDGMENTS

This research was supported by the international research project, Localization and Identification Of moving Noise sources (LION). The Swiss contribution was funded by the Swiss National Science Foundation (Grant No. 185530). The German contribution was funded by the German Research Foundation (Grant No. 422372636).

Arntzen, M., and Simons, D. G. (**2014**). "Modeling and synthesis of aircraft flyover noise," Appl. Acoust. **84**, 99–106.
Attenborough, K., and Renterghem, T., eds. (**2021**). *Predicting Outdoor Sound*, 2nd ed. (CRC Press, Boca Raton, FL).
Brooks, T. F., and Humphreys, W. M. (**2006**). "A deconvolution approach for the mapping of acoustic sources (DAMAS) determined from phased microphone arrays," J. Sound Vib. **294**(4), 856–879.

Collier, S., and Wilson, D. (**2003**). "Performance bounds for passive sensor arrays operating in a turbulent medium: Plane-wave analysis," J. Acoust. Soc. Am. **113**(5), 2704–2718.

Forssén, J., Hoffmann, A., and Kropp, W. (**2018**). "Auralization model for the perceptual evaluation of tyre–road noise," Appl. Acoust. **132**, 232–240.

Guérin, S., and Siller, H. (**2008**). "A hybrid time-frequency approach for the source localization analysis of acoustic fly-overs," in *14th AIAA/CEAS Aeroacoustics Conference (29th AIAA Aeroacoustics Conference)*, May 5–7, Vancouver, British Columbia, Canada, paper AIAA 2008-2955.

Guérin, S., and Weckmüller, C. (**2008**). "Frequency-domain reconstruction of the point-spread function for moving sources," in *Proceedings of the 2nd Berlin Beamforming Conference (BeBeC),* Berlin, Germany [Gesellschaft zur Förderung angewandter Informatik (GFaI), Berlin], paper BeBeC-2008-14, available at http://www.bebec.eu/Downloads/BeBeC2008/Papers/BeBeC-2008-14_Guerin_Weckmueller.pdf (Last viewed January 11, 2023).

Guérin, S., Weckmüller, C., and Michel, U. (**2006**). "Beamforming and deconvolution for aerodynamic sound sources in motion," in *Proceedings of the 1st Berlin Beamforming Conference (BeBeC),* Berlin, Germany, November 21–22, 2006 [Gesellschaft zur Förderung angewandter Informatik (GFaI), Berlin], paper BeBeC-2006-16, available at http://www.bebec.eu/Downloads/BeBeC2006/Papers/BeBeC-2006-16_Guerin_Weckmueller_Michel.pdf (Last viewed January 11, 2023).

Habets, E., Cohen, I., and Gannot, S. (**2008**). "Generating nonstationary multisensor signals under a spatial coherence constraint," J. Acoust. Soc. Am. **124**(5), 2911–2917.

International Civil Aviation Organization. (**2017**). "ANNEX 16 to the convention on international civil aviation, environmental protection," *Volume I - Aircraft Noise*, 8th ed., https://store.icao.int/en/annex-16-environmental-protection-volume-i-aircraft-noise (Last viewed January 11, 2023).

Ishii, Y., Hald, J., Ishii, T., Oinuma, H., Nagai, K., Yokokawa, Y., and Yamamoto, K. (**2014**). "High-resoluation fly-over beamforming using a practical array," in *Proceedings of the 5th Berlin Beamforming Conference (BeBeC),* Berlin, Germany, 2014, paper BeBeC-2014-16, available at http://bebec.eu/Downloads/BeBeC2014/Papers/BeBeC-2014-16.pdf.

ISO 9613-1:1993, "Acoustics—Attenuation of sound during propagation outdoors—Part 1: Calculation of the absorption of sound by the atmosphere" (International Organization for Standardization, Geneva, Switzerland, **1993**).

Kamrath, M. J., Ostashev, V. E., Wilson, D. K., White, M. J., Hart, C. R., and Finn, A. (**2021**). "Vertical and slanted sound propagation in the near-ground atmosphere: Amplitude and phase fluctuations," J. Acoust. Soc. Am. **149**(3), 2055–2071.

Laakso, T. I., Välimäki, V., Karjalainen, M., and Laine, U. K. (**1996**). "Splitting the unit delay [FIR/all pass filters design]," IEEE Signal Process. Mag. **13**(1), 30–60.

Merino-Martínez, R., Sijtsma, P., Snellen, M., Ahlefeldt, T., Antoni, J., Bahr, C., Blacodon, D., Ernst, D., Finez, A., Funke, S., Geyer, T., Haxter, S., Herold, G., Huang, X., Humphreys, W., Leclère, Q., Malgoezar, A., Michel, U., Padois, T., Pereira, A., Picard, C., Sarradj, E., Siller, H., Simons, D., and Spehr, C. (**2019**). "A review of acoustic imaging methods using phased microphone arrays," CEAS Aeronaut. J. **10**(1), 197–230.

Michel, U., Barsikow, B., Böhning, P., and Hellming, M. (**2004**). "Localisation of sound sources on moving vehicles with phased microphone arrays," in *Proceedings of the 33rd International Congress and Exposition on Noise Control Engineering (InterNoise)*, Prague, Czech Republic, August 22–25, 2004. pp. 4069–4075.

Michel, U., and Möser, M. (**2009**). "Akustische Antennen" ("Acoustics antennas"), in *Messtechnik der Akustik (Measurement Technology of Acoustics)*, edited by M. Möser (Springer Berlin Heidelberg, Berlin, Heidelberg), pp. 365–425.

Mirabilii, D., Schlecht, S. J., and Habets, E. A. P. (**2021**). "Generating coherence-constrained multisensor signals using balanced mixing and spectrally smooth filters," J. Acoust. Soc. Am. **149**(3), 1425–1433.

Ostashev, V., Collier, S., and Wilson, D. (**2009**). "Transverse-longitudinal coherence function of a sound field for line-of-sight propagation in a turbulent atmosphere," Waves Random Complex Media **19**(4), 670–691.

Ostashev, V., and Wilson, D. (**2016**). *Acoustics in Moving Inhomogeneous Media*, 2nd ed. (CRC Press, Taylor & Francis Group, Boca Raton, FL).

Ostashev, V. E., Kamrath, M. J., Wilson, D. K., White, M. J., Hart, C. R., and Finn, A. (**2021**). "Vertical and slanted sound propagation in the near-ground atmosphere: Coherence and distributions," J. Acoust. Soc. Am. **150**(4), 3109–3126.

Pieren, R., Bertsch, L., Lauper, D., and Schäffer, B. (**2019**). "Improving future low-noise aircraft technologies using experimental perception-based evaluation of synthetic flyovers," Sci. Total Environ. **692**, 68–81.

Pieren, R., and Lincke, D. (**2022**). "Auralization of aircraft flyovers with turbulence-induced coherence loss in ground effect," J. Acoust. Soc. Am. **151**(4), 2453–2460.

Piet, J.-F., Michel, U., and Böhning, P. (**2002**). "Localization of the acoustic sources of the A340 with a large phased microphone array during flight tests," in *8th AIAA/CEAS Aeroacoustics Conference and Exhibit*, June 17–19, Breckenridge, CO, paper AIAA 2002-2506.

Pires, L., Dougherty, R., Gerges, S., and Catalano, F. (**2012**). "Predicting turbulent decorrelation in acoustic phased arrays," in *50th AIAA Aerospace Sciences Meeting including the New Horizons Forum and Aerospace Exposition*, January 9–12, Nashville, Tennessee.

Rietdijk, F., Forssén, J., and Heutschi, K. (**2017**). "Generating sequences of acoustic scintillations," Acta Acust. united Acust. **103**(2), 331–338.

Rizzi, S., LeGriffon, I., Pieren, R., and Lothar Bertsch, L. (**2020**). "A comparison of aircraft flyover auralizations by the aircraft noise simulation working group," in *AIAA Aviation 2020 Forum*, June 15-19 (Virtual Event).

Rizzi, S. A., and Sahai, A. K. (**2019**). "Auralization of air vehicle noise for community noise assessment," CEAS Aeronaut. J. **10**(1), 313–334.

Sijtsma, P. (**2007**). "Beamforming on moving sources," Report No. NLR-TP-2006-733, National Aerospace Laboratory, available at https://core.ac.uk/download/pdf/53034218.pdf (Last viewed January 11, 2023).

Siller, H., Schumacher, T., and Hage, W. (**2020**). "Analysis of the jet noise emitted by an aircraft during take-off," in *Proceedings of the 8th Berlin Beamforming Conference (BeBeC)*, Berlin, Germany [Gesellschaft zur Förderung angewandter Informatik (GFaI), Berlin], paper BeBeC-2020-S03, available at https://www.bebec.eu/fileadmin/bebec/downloads/bebec-2020/papers/BeBeC-2020-S03.pdf (Last viewed January 11, 2023).

Siller, H., Schumacher, T., and Hage, W. (**2021**). "Low noise ATRA - phased array measurements of jet noise in flight," in *AIAA AVIATION 2021 Forum*, August 2–6, 2021 (Virtual Event), paper AIAA 2021-2160.

Virtanen, P., Gommers, R., Oliphant, T. E., Haberland, M., Reddy, T., Cournapeau, D., Burovski, E., Peterson, P., Weckesser, W., Bright, J., van der Walt, S. J., Brett, M., Wilson, J., Millman, K. J., Mayorov, N., Nelson, A. R. J., Jones, E., Kern, R., Larson, E., Carey, C. J., Polat, İ., Feng, Y., Moore, E. W., VanderPlas, J., Laxalde, D., Perktold, J., Cimrman, R., Henriksen, I., Quintero, E. A., Harris, C. R., Archibald, A. M., Ribeiro, A. H., Pedregosa, F., and van Mulbregt, P. and SciPy 1.0 Contributors. (**2020**). "SciPy 1.0: Fundamental algorithms for scientific computing in Python," Nat. Methods **17**, 261–272.

Vorländer, M. (**2020**). *Auralization: Fundamentals of Acoustics, Modelling, Simulation, Algorithms and Acoustic Virtual Reality*, 2nd ed. (Springer, Cham, Switzerland).

Wilson, D. (**1998**). "Performance bounds for acoustic direction-of-arrival arrays operating in atmospheric turbulence," J. Acoust. Soc. Am. **103**(3), 1306–1319.